

Article

Dynamic Modeling and Passivity-Based Control of an RV-3SB Robot

Manuel Cardona ^{1,†}, Fernando E. Serrano ^{2,*,†} and Cecilia E. García Cena ^{3,†}¹ Research Department, Universidad Don Bosco, San Salvador 1874, El Salvador; manuel.cardona@udb.edu.sv² Instituto de Investigación en Energía IIE, Universidad Nacional Autónoma de Honduras UNAH, Tegucigalpa 11101, Honduras³ Centre for Automation and Robotics (CAR), Universidad Politécnica de Madrid (UPM), 28012 Madrid, Spain; cecilia.garcia@upm.es

* Correspondence: serranofer@eclipseo.eu

† These authors contributed equally to this work.

Abstract: This paper shows the dynamic modeling and design of a passivity-based controller for the RV-3SB robot. Firstly, the dynamic modeling of a Mitsubishi RV-3SB robot is conducted using Euler–Lagrange formulation in order to obtain a decoupled dynamic model, considering the actuator orientation besides the position of the analyzed robot. It is important to remark that the dynamic model of the RV-3SB robot is conducted based on kinematic model obtention, which is developed by the implementation of screw theory. Then, the passivity-based controller is obtained by separating the end effector variables and the actuator variables by making an appropriate coordinate transformation. The passivity-based controller is obtained by selecting an appropriate storage function, and by using Lyapunov theory, the passivity-based control law is obtained in order to drive the error variable, which is the difference between the measured end effector position variable and the desired end effector position variable. The passivity-based controller makes the error variable reach the origin in finite time, taking into consideration the dissipation properties of the proposed controller in order to stabilize the desired end effector position. A numerical simulation experiment is performed in order to validate the theoretical results obtained in this research. Using numerical experimentation, it is verified that the proposed control strategy is efficient and effective in driving the error variable to the origin in comparison with other modified techniques found in the literature. Finally, an appropriate discussion and conclusion of this research study are provided.



Citation: Cardona, M.; Serrano, F.E.; García Cena, C.E. Dynamic Modeling and Passivity-Based Control of an RV-3SB Robot. *Actuators* **2023**, *12*, 339. <https://doi.org/10.3390/act12090339>

Academic Editor: Zhuming Bi

Received: 2 June 2023

Revised: 31 July 2023

Accepted: 10 August 2023

Published: 23 August 2023



Copyright: © 2023 by the authors. Licensee MDPI, Basel, Switzerland. This article is an open access article distributed under the terms and conditions of the Creative Commons Attribution (CC BY) license (<https://creativecommons.org/licenses/by/4.0/>).

Keywords: dynamic output feedback control; robotics; passivity-based control

1. Introduction

Industrial robots have been extensively implemented for several decades, with different applications of their mechanisms in operations like drilling, painting, screwing and welding across different industrial environments. It is important to mention that industrial robots are classified into two main categories: serial robots and parallel robots. Serial robots are the type of robots in which each link is connected to the other, successively, and parallel robots are those in which each link is connected in a parallel fashion. Among the most important serial robots implemented for industrial environments are the many types of six-degree-of-freedom mechanisms used for different tasks. Meanwhile, parallel robots, which are commonly implemented in different kinds of industrial applications, include the delta robot and the Stewart–Gough platform, which provide the necessary degrees of freedom (DOF) and flexibility in comparison with serial robots.

As we know, serial robots are implemented and studied due to the importance they have in the implementation of different mechanisms across different tasks, increasing productivity and reliability on assembly lines. Nevertheless, it is important to remark that

many experimental robots are currently being developed, taking into consideration the necessity for new kinematic and dynamic analyses. Additionally, novel control strategies need to be designed to obtain optimal performance for trajectory tracking of the end effector, especially in diverse industrial applications. For these reasons, it is important to analyze the kinematic and dynamic properties of experimental or laboratory robotic manipulators in order to provide relevant theoretical, experimental, and practical conclusions about any type of implementation of robot manipulators.

Kinematics plays an important role in the mathematical modeling of robot manipulators. There are many kinematic model methodologies that define the direct and inverse kinematics of a robot manipulator. Among these strategies are the Denavit–Hartenberg convention, Hamilton quaternions, and screw theory. It is crucial to mention the following research papers in which these kinematic model methodologies are found. So, for example, in [1], a novel inverse kinematic model was utilized for a novel 6R manipulator by implementing quaternions. Additionally, in [2], the kinematics of a parallel robot were evinced using lie group theory. Other interesting results are found in papers like [3], in which the forward kinematics of robot-assisted surgery are presented. Moreover, in [4], the kinematic reliability of an industrial robots is evinced. In [5], a forward kinematics analysis of a general Stewart–Gough platform using a multibody formulation is performed; in [6], a 7R six-degree-of-freedom robot with a non-spherical wrist kinematic calibration procedure is presented. Furthermore, another interesting piece of research is shown in [7], in which the kinematic calibration of a 5-DOF machining robot is performed using the Kalman filter approach. All these results are important to the present study, taking into consideration that they provide the theoretical framework for the analyzed robotic mechanisms. It is important to consider that in the above-mentioned research studies, there are some strategies, such as quaternions, that are very important to the design of a kinematic model for an RV-3SB robot using screw theory.

One of the main issues on which the present paper is focused is the dynamic modeling of an RV-3SB robot. The approach used in this research study presents their fundamentals utilizing an Euler–Lagrange approach, but considering the kinematic model obtained by screw theory for the analyzed robots, it is important to consider that the dynamic model derivation is significantly reduced, which is a must when dynamic model derivation for a new robotic mechanism is obtained. The following references are important for the present study, taking into consideration the contribution to the dynamic model derivation of the RV-3SB robot. For example, in [8], bi-stable dynamics in a two-module vibration-driven robot are presented. Additionally, in [9], the dynamics equations of a Hexabot robot are obtained using the Lagrange equation of a second kind. Furthermore, in [10], neural dynamics-driven control of a redundant robot is provided. In [11], remote teaching of dynamics and control of robots is performed. Other studies that have provided significant results can be found in papers such as [12,13], according to the dynamic model mathematical derivation for different types of robots. The implementation of different dynamic model techniques in the above studies is an important contribution to the present paper, considering that dynamic models based on the Euler–Lagrange formulation are significant for the dynamic model derivation of the RV-3SB robot analyzed in this research.

Screw theory is fundamental to the derivation of feasible kinematic models for forward kinematics and inverse kinematics; for this reason, it is important to mention the following studies. For example, in [14], a complete review of screw theory for the kinematic modeling of serial and parallel robots is presented. In this chapter, it is stressed that reciprocal screw theory facilitates obtaining compact and elegant kinematic model representations for the previously mentioned types of robots. Meanwhile, in [15], it is shown how screw theory is implemented for a force model of a crane. In [16], a configuration synthesis of deployable antennas based on screw theory is proposed. Another interesting paper that is worthy of citation is found in [17], in which a higher-order representation of metamorphic mechanisms based on screw theory is presented. In [18], screw theory is used to conduct a vibration analysis of a space parallel robot. Furthermore, in [19], a mobility analysis

of scissor-like elements is presented via the implementation of reciprocal screw theory. As we know, the screw consists of defining the velocities and moment or force vectors which represents the rotation about an specified axis. Screw theory provides a compact and simplified model that is used for the forward and inverse kinematics derivations of our studied and analyzed robot. The previous cited research results provides the mathematical fundamentals for this research study.

Nowadays, there is a vast amount of control strategies for different types of robots, which are independent if they are serial chain or parallel chain configurations. Therefore, it is important to mention several research studies related to this topic in order to provide an introductory theoretical framework for the passivity-based control strategy of the RV-3SB robot. Among the papers found in the scientific literature, [20] presents the visual control of a robot using a Deep Reinforcement Learning technique. In [21] the control of a laparoscopic robot is performed using a leap motion sensor. In [22], the coordinated control of a space robot manipulator is evinced. Another interesting result is shown in [23], in which the robust variable admittance control of a human–robot manipulator is shown. In [24], a non-singular terminal sliding mode controller for a prosthetic leg robot is described. Ultimately, in [25], the robust control of a planar snake robot using Takagi–Sugeno fuzzy control is presented.

Passivity-based control is the main control strategy implemented in this research study, so it is worth mentioning the following passivity-based control strategies. In [26] the control of a piezoelectric actuator is achieved using a Krasovskii passivity-based approach. Then, in [27], the instability problem caused by the constant power load in a Buck converter is addressed. Other important results are found in papers such as [28], in which a self-balancing robot is controlled by a proportional–integral–derivative (PID) passivity-based control strategy. In [29], an underactuated three-dimensional crane is controlled by a passivity-based controller. Then, in [30], a three degrees of freedom 3-DOF crane is controlled using a passivity-based adaptive trajectory tracking controller. Finally in [31], a spacecraft attitude simulator is controlled using a passivity-based sliding mode controller. Passivity-based control, as we know, consists of a control strategy based on the energy consideration of the nonlinear dynamic system to be controlled. It is important to mention that this is the main control strategy for this research paper. This strategy is novel and considers the energy properties of the nonlinear dynamics of the RV-3SB robot mechanism.

In this paper, we propose the passivity-based control of a Mitsubishi RV-3SB robot. First, the kinematic model of the robot with the implementation of screw theory is obtained. Then, the dynamic model of the robot manipulator is obtained via the implementation of the Euler–Lagrange formulation, yielding a decoupled non-linear dynamic model for the position and orientation of the Mitsubishi RV-3SB robot. The passivity-based controller of the robot is then obtained by selecting a suitable storage function. This choice ensures that the passivity-based condition is met by implementing the selected control law, thereby satisfying the closed-loop stability requirements. It is important to remark that the passivity controller consists of the passivity-based control law along with a output feedback controller, allowing it to achieve the desired trajectory tracking system performance. A numerical experiment is conducted in order to validate the theoretical results provided in this research study. Finally, a discussion and conclusion section is presented to discuss the results of this research study.

The advantages of the proposed controller, as demonstrated in this research study, are summarized in comparison to other control strategies found in the literature, as follows:

- The passivity-based control law is relatively simple in comparison with other strategies found in the literature.
- Considering that this control strategy is novel and has not been found in the literature, it offers a suitable approach to solving this kind of problem.
- Naturally, dynamical systems established in the Lagrangian and Hamiltonian mathematical representations possess energy considerations. Therefore, the passivity-based

controller proposed in this paper offers an appropriate control strategy, taking into account the dynamics of the RV-3SB robot.

- As verified experimentally and theoretically, the passivity-based control strategy presented in this paper yields a better closed loop performance in comparison with other control strategies.
- The passivity-based controller evinced in this research study yields a better low computational effort considering the implementation in real-time hardware such as hardware in the loop.
- The parameters of this passivity-based controller are easy to tune with some evolutionary and/or optimization algorithm. This will be considered as a future direction of this research study.

Table 1 shows a qualitative comparative analysis of four control strategies for robotic manipulators. These are the most relevant references mentioned in this research study, so it is important to evince this comparative analysis that will be corroborated later in the numerical simulation section. The advantages and disadvantages of these control techniques are presented in order to demonstrate the weakness and strengths of these control approaches.

Table 1. Qualitative comparative analysis of the most relevant references.

Controller Approach	Advantage	Disadvantage
Chan Zheng et al., 2021 [32]	This control approach provides an identification of linear damping.	Disturbances and especially unmodeled dynamics are not considered.
Nguyen et al., 2021 [33]	Proportional integral control PID along with passivity-based controller provides a robust control approach.	Parameter tuning is not considered in this research study.
Gandarilla et al., 2021 [28]	PID controller along with passivity-based controller is more precise and robust considering the well-known performance of PID controller and the energy consideration of a passivity-based controller.	The PID controller part must be tuned carefully in order to obtain an optimal performance in comparison with a standalone passivity-based controller.
Shen et al., 2021 [30]	The passivity-based adaptive controller for the 3-DOF overhead crane provides a better performance in comparison with a non-adaptive controller.	The adaptive passivity-based control law increase the computational effort.

This paper is divided into the following sections: in Section 2, the relevant related work is presented; meanwhile, in Section 3, the theoretical derivations of the dynamic model of the robot and the control strategy are presented; then, in Section 4, two numerical experiments are performed; finally, in Sections 5 and 6, the discussion and conclusions of this research strategy are presented.

2. Related Work

This section provides a comprehensive review of closely related work in order to demonstrate the importance of the present research study. This section is focused on the following issues, which are important in order to evince a detailed overview of the most relevant research studies found in the scientific literature:

- Kinematics.
- Industrial robotics.
- Dissipative dynamic systems.
- Passivity-based control.

- Diverse control strategies for robotics.

To begin this literature review, we start with some kinematics techniques for industrial robots, taking into consideration that in this present research study, the screw theory is considered for both the kinematic and dynamic modeling of the RS-3SB robot. For instance, in [34], a differential kinematic modeling of a mobile robot is presented. Meanwhile, in [35], a kinematic workspace model of 3R, 4R, 5R, or 6R robots is presented. Then, in [36], the meaning of four co-reciprocal screws is presented in terms of its kinematic significance. In [37], the identification of kinematics parameters of a multi-link manipulator is presented. Furthermore, several other research studies explore the kinematics of diverse types of robotic manipulators. For instance, in [38], a new formulation of the inverse dynamic of a parallel delta robot is provided. Similarly, in [39], a closed form for inverse dynamic model of the delta parallel robot is presented.

Other interesting strategies for kinematic modeling of serial and parallel robots are found in papers such as [40], in which Clifford algebra is implemented for kinematic control of a serial robot. Then, in [41], an automatic approach to identify the parameters of a serial link chains using reciprocal screws is presented. Meanwhile, in [42], screw theory and dual quaternions are used for motion controllers. In [43], conformal geometric algebra is implemented in order to obtain the inverse kinematic of serial robots. Furthermore, in [7], an extended Kalman filter is implemented in order to obtain the kinematic calibration of a 5-DOF hybrid machining robot. Finally, in [1], the inverse kinematic formula for a new class of 6R robot is presented.

Industrial and many kinds of novel robot manipulators are crucial to mention in this research paper, taking into consideration the results that are important to the present research study. For instance, in papers such as [44], a bipedal walking robot is shown. Other interesting results are found in [45], in which a model control for industrial robots is presented. In [46], the adaptive output feedback tracking control of a non-holonomic mobile robot is presented. Meanwhile, in [47], a control strategy for two link underactuated planar robots is presented. In [48], a stable controller for a robot manipulator is evinced.

Dissipation properties of nonlinear dynamics systems are important, considering the characteristics of passivity-based controllers. For instance, in [49], the dissipative characteristics of a negative imaginary system are exploited in order to design a control strategy. In [50], the dissipative properties required for infinite dimensional continuous control are studied. Meanwhile, in [51], the dissipative output feedback control of Markovian jump systems is presented. In [52], the dissipative optimal infinite dimensional control is studied. Furthermore, interesting results are found in [30], in which dissipative discrete time stochastic delayed systems are analyzed. Finally, a discrete-time neural network and its dissipative control are designed in [53].

Passivity-based control is one of the control strategies developed for various types of physical systems, including electrical and mechanical systems. As mentioned earlier, this strategy involves selecting a storage function to ensure that the chosen control law satisfies the passivity requirements. In [54] the passivity and power-based control of a robot is presented; in [55], the adaptive passivity-based force controller for an uncertain system is studied; in [56], the passivity-based control of hydraulic robots is evinced. Furthermore, a distributed passivity-based controller for constrained robotics networks is shown in [57], and in [58], new results in passivity-based control for robots are presented. Finally, other control strategies such as backstepping control, sliding mode control, output feedback robust control, among others, can be found in [23,59–63].

3. Dynamic Modeling of the RV-3SB Robot Manipulator and Controller Design

The dynamic modeling of the RV-3SB (Figure 1) robot is presented in this section. In order to obtain a simple dynamic model, the Euler–Lagrange formulation is applied in this section. Considering that the last three axes of the robot intersect each other, the dynamic model of this robot is decoupled, which implies that the robot's position and orientation can be analyzed independently. Furthermore, this dynamic model formulation is suitable

for trajectory tracking controller design, as verified in the control design section. Consider the following kinetic and potential energy functions:

$$\begin{aligned}
 K &= \frac{1}{2} \dot{q}^T I \dot{q} + \frac{1}{2} \dot{X}^T M \dot{X} \\
 P &= mg \epsilon^T X
 \end{aligned}
 \tag{1}$$

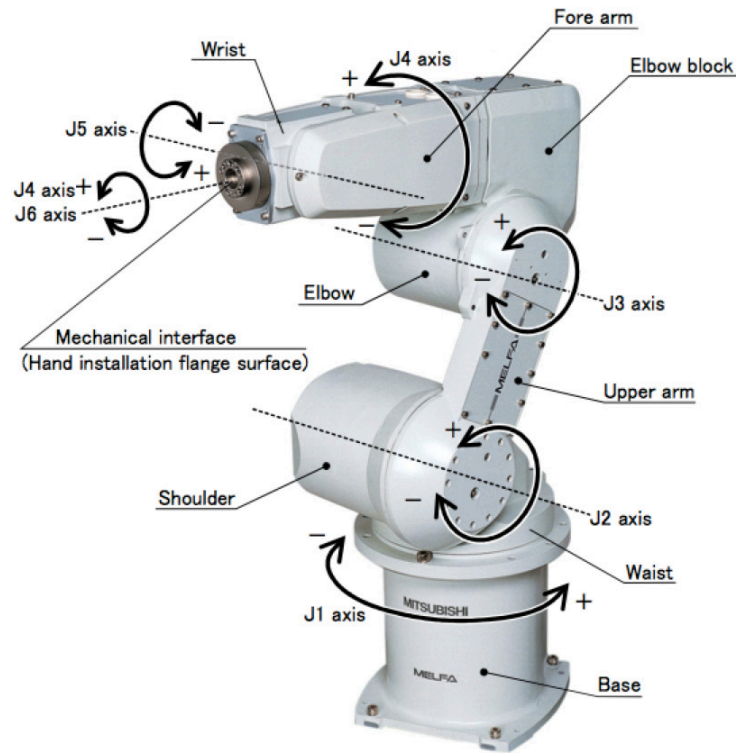


Figure 1. The RV-3SB Mitsubishi serial robot with 6 Degrees of Freedom.

In which I is the inertia matrix, M is the mass matrix, g is the gravity constant, and $m = \sum_{i=1}^6 m_i$ is the total mass of the robot, as stated below:

$$\begin{aligned}
 I &= \begin{bmatrix} I_1 & 0 & 0 & 0 & 0 & 0 \\ 0 & I_2 & 0 & 0 & 0 & 0 \\ 0 & 0 & I_3 & 0 & 0 & 0 \\ 0 & 0 & 0 & I_4 & 0 & 0 \\ 0 & 0 & 0 & 0 & I_5 & 0 \\ 0 & 0 & 0 & 0 & 0 & I_6 \end{bmatrix} \\
 M &= \begin{bmatrix} m & 0 & 0 \\ 0 & m & 0 \\ 0 & 0 & m \end{bmatrix}
 \end{aligned}
 \tag{2}$$

with the following vectors:

$$\begin{aligned}
 q &= [\theta_1, \theta_2, \theta_3, \theta_4, \theta_5, \theta_6]^T \\
 \epsilon &= [0, 1, 0]^T \\
 X &= [x, y, z]^T
 \end{aligned}
 \tag{3}$$

In which θ_i , for $i = 1 \dots 6$, are the actuator angles, and x, y and z are the end effector coordinates. Basically, the vector q is related to the orientation and X is related to the position of the designed robot. Consider the following Lagrangian:

$$\mathcal{L} = K - P = \frac{1}{2}\dot{q}^T I \dot{q} + \frac{1}{2}\dot{x}^T M \dot{X} - mg\epsilon^T X \quad (4)$$

Now consider the Euler–Lagrange formulation:

$$\begin{aligned} \frac{d}{dt} \left[\frac{\partial \mathcal{L}}{\partial \dot{q}} \right] - \frac{\partial \mathcal{L}}{\partial q} &= \tau_q \\ \frac{d}{dt} \left[\frac{\partial \mathcal{L}}{\partial \dot{X}} \right] - \frac{\partial \mathcal{L}}{\partial X} &= F_v \end{aligned} \quad (5)$$

obtaining the following dynamic system:

$$\begin{aligned} I\ddot{q} &= \tau_q \\ M\ddot{X} + mg\epsilon^T &= F_v \end{aligned} \quad (6)$$

Or in other way:

$$I\ddot{Q} = \underbrace{\tau_q}_{\tau_1} \quad (7)$$

In which $Q = q, F_v \in \mathbb{R}^3$ is a virtual force and $\tau_q \in \mathbb{R}^6$ is the actuator torques. So, the previous equation can be transformed into a state space formulation as follows:

$$\begin{aligned} \dot{Q}_1 &= Q_2 \\ \dot{Q}_2 &= D^{-1}\tau \end{aligned} \quad (8)$$

For $Q_1 = Q, Q_2 = \dot{Q}$ and $\tau = \tau_1$ with the following matrix:

$$D = I \quad (9)$$

The parameters of the robot are given in the following paragraph, as shown in the paper [64]

- Six Degrees of Freedom.
- Repeatability: ± 0.02 mm.
- Maximum speed: 5500 mm/s.
- Range of Motion (degrees): $J_1 = 340, J_2 = 225, J_3 = 191, J_4 = 320, J_5 = 240, J_6 = 720$.
- Maximum speed in each joint (deg/seg): $J_1 = 250, J_2 = 187, J_3 = 250, J_4 = 412, J_5 = 412, J_6 = 660$.
- Weight: 37 kg.

It is important to remark that the kinematic model of this robot is obtained via screw theory; the following screws are defined in Table 2 as shown in [64]:

Table 2. Screw axis Location of the RV-3SB robot.

Joint i	Screw Axis (S_i)	Screw Axis Location (S_{0i})
J_1	$[0, 0, 1]$	$[0, 0, 0]$
J_2	$[0, 1, 0]$	$[95, 0, 350]$
J_3	$[0, 1, 0]$	$[95, 0, 595]$
J_4	$[0, 0, 1]$	$[-40, 0, 0]$
J_5	$[0, 1, 0]$	$[-40, 0, 865]$
J_6	$[0, 0, 1]$	$[-40, 0, 0]$

Passivity-Based Control of the RV-3SB Robot Manipulator

For the passivity-based control strategy of the RV-3SB robot manipulator, the required energy considerations are taken into account in order to ensure the closed loop stability. It is important to recall that passivity-based control is an important technique for robotic systems that has been implemented over decades for different types of mechanisms. To obtain the obtained passivity-based control law consider the following theorem:

Theorem 1. *The dynamic model of the robot RV-3SB (7) represented in the state-space model, as appears in (8), is passive if the following control law is implemented:*

$$\begin{aligned}\tau &= -DR_2^{-1}R_1Q_1 - DR_2^{-1}\frac{Q_2}{\|Q_2\|^2}e^T\dot{Y}_{ref} \\ &+ DR_2^{-1}\frac{Q_2}{\|Q_2\|^2}e^TY + DR_2^{-1}\frac{Q_2}{\|Q_2\|^2}\tau_p^TY\end{aligned}\quad (10)$$

In which the error variable is given as follows:

$$e = Y_{ref} - Y \quad (11)$$

Y_{ref} is the reference variable for trajectory tracking purposes, and $Y = [x, y, z]^T$. The matrices gains are defined as $R_1 \in \mathbb{R}^{6 \times 6}$ and $R_2 \in \mathbb{R}^{6 \times 6}$. The control input τ_p is given by $\tau_p = K_p Y$ in which $K_p \in \mathbb{R}^{3 \times 3}$ is a gain matrix.

Proof. Consider the following Lyapunov functional:

$$V = \frac{1}{2}Q_1^TR_1Q_1 + \frac{1}{2}Q_2^TR_2Q_2 + \frac{1}{2}e^Te \quad (12)$$

By obtaining the first derivative of the previous Lyapunov functional and making the appropriate substitutions, we yield:

$$\begin{aligned}\dot{V} &= Q_1^TR_1\dot{Q}_1 + Q_2^TR_2D^{-1}\dot{\tau} \\ &+ e^T\dot{Y}_{ref} - e^T\dot{Y}\end{aligned}\quad (13)$$

Then, by substituting (10) into (13), we obtain:

$$\dot{V} \leq \tau_p^TY \quad (14)$$

Thus, the system is passive and stable and the proof is completed. \square

Now, in order to obtain the virtual force input F_v , the following property is necessary.

Property 1. *Consider the following transformation matrices [64] $T_i \forall i = 1, \dots, 6$ in which the following matrices establish the necessary coordinate transformation to each axis:*

$$\begin{aligned}G_6 &= T_1.T_2.T_3.T_4.T_5.T_6 \\ G_5 &= T_1.T_2.T_3.T_4.T_5 \\ G_4 &= T_1.T_2.T_3.T_4 \\ G_3 &= T_1.T_2.T_3 \\ G_2 &= T_1.T_2 \\ G_1 &= T_1\end{aligned}\quad (15)$$

Then, considering that the control input vector is given by $\tau = [\tau_{u1}, \tau_{u2}, \tau_{u3}, \tau_{u4}, \tau_{u5}, \tau_{u6}]^T$ and the input vector is given by $F_v = [F_{vx}, F_{vy}, F_{vz}]^T$; the virtual control input F_v is found by solving the following system of equations:

$$\begin{bmatrix} F_v \\ F_v \\ F_v \\ F_v \\ F_v \\ F_v \end{bmatrix} = \begin{bmatrix} G_6(1 : 3, 4)^T & 0_3 & 0_3 & 0_3 & 0_3 & 0_3 \\ 0_3 & G_5(1 : 3, 4)^T & 0_3 & 0_3 & 0_3 & 0_3 \\ 0_3 & 0_3 & G_4(1 : 3, 4)^T & 0_3 & 0_3 & 0_3 \\ 0_3 & 0_3 & 0_3 & G_3(1 : 3, 4)^T & 0_3 & 0_3 \\ 0_3 & 0_3 & 0_3 & 0_3 & G_2(1 : 3, 4)^T & 0_3 \\ 0_3 & 0_3 & 0_3 & 0_3 & 0_3 & G_1(1 : 3, 4)^T \end{bmatrix}^{-1} \begin{bmatrix} \tau_{u1} \\ \tau_{u2} \\ \tau_{u3} \\ \tau_{u4} \\ \tau_{u5} \\ \tau_{u6} \end{bmatrix} \quad (16)$$

In which $G_i(1 : 3, 4) \forall i = 1, \dots, 6$ is the fourth column of the transformation matrices, meanwhile, 0_3 is a zero row vector of three elements. The inverse of the matrix which appears in (16) is solved by the Moore–Penrose pseudo-inverse.

4. Numerical Experiment

In this section, two numerical experiments are presented, taking into consideration the simulation parameters and the conditions given in Section 3. The two numerical examples consist of the trajectory tracking of the Mitsubishi RV-3SB robot using different trajectory profiles, as explained below:

- A sigmoidal reference profile.
- A sinusoidal reference profile.

The results obtained using the proposed control strategy are compared with two strategies found in the literature, as demonstrated in the content of this section. The controller parameters of the proposed control strategy are presented in Table 3:

Table 3. Mitsubishi RV-3SB robot parameters for experiment 1 and experiment 2.

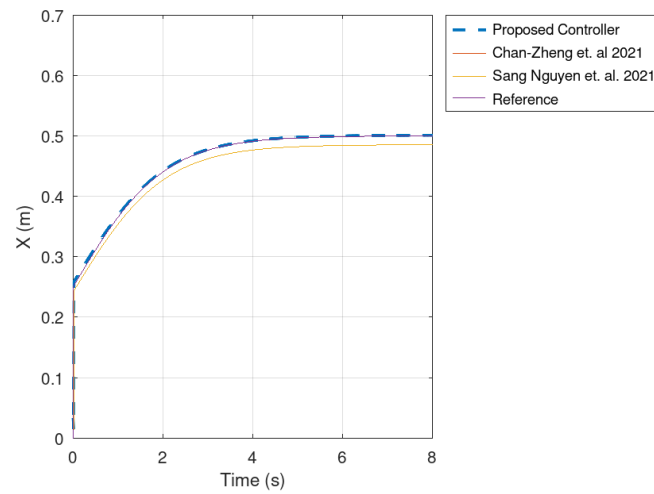
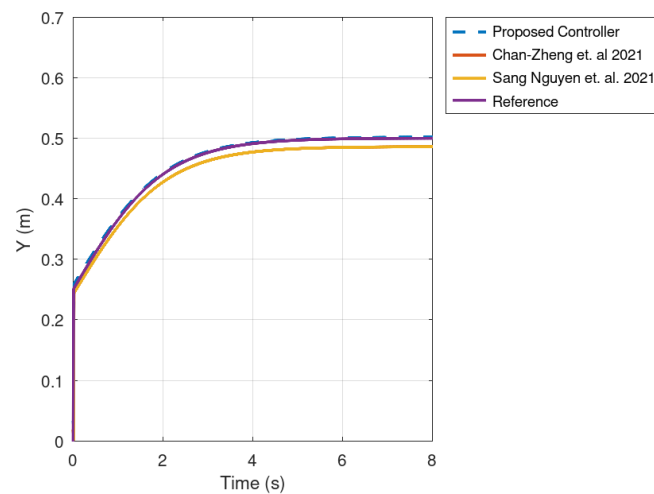
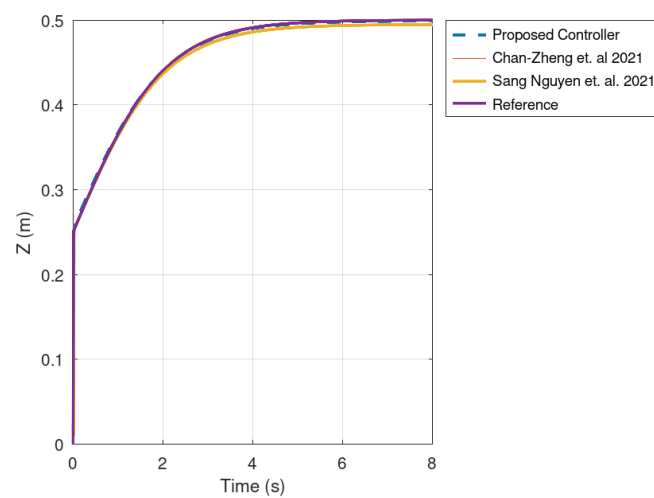
Parameter	Parameter Value
R_1	$I_6 \times 8 \times 10^{-1}$
R_2	$I_6 \times 10 \times 10^{-1}$
K_p	$I_3 \times 1 \times 10^{-1}$

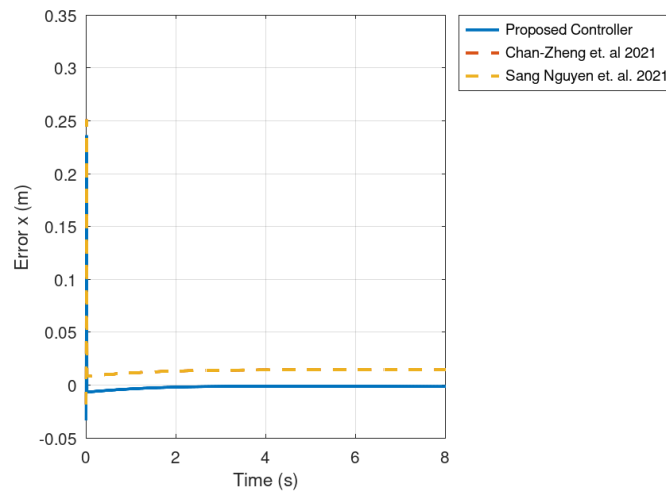
4.1. Experiment 1

This experiment is performed using a sigmoidal function as the reference signal. The main purpose of this experiment is to validate that the tracking error, resulting from the proposed control strategy, converges to zero within a finite time frame. The gain matrices are selected to ensure that the variables achieve optimal performance, clarifying that closed loop stability is ensured independently of the initial conditions of the robot’s dynamic system. The results are compared with two control strategies [32,33] in order to obtain conclusions about the results.

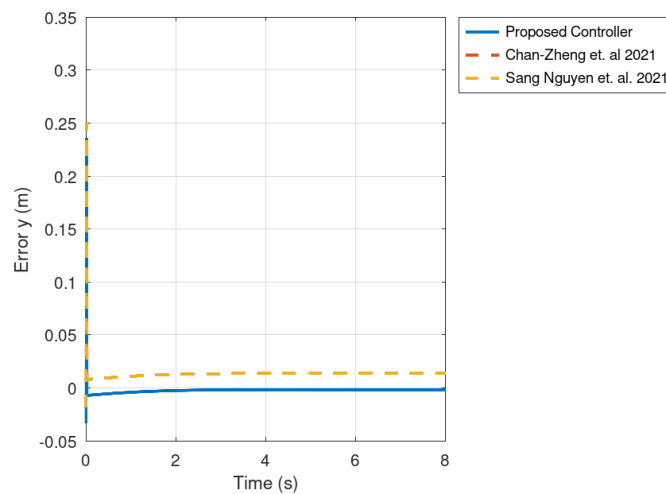
In Figures 2 and 3 the evolution over time of the variables x , y and z , along with their respective errors, is presented. It is important to note that the results obtained using the proposed controller are improved by the proposed control strategy. As verified later, the integral square error ISE obtained with the proposed method is significantly smaller than that obtained using the other previously reported methods [32,33].

Figures 4 and 5 illustrate the actuator torques of the Mitsubishi RV-3SB robot. It can be noticed that the actuator torques reach the origin in finite time more quickly. This behavior is attributed to the passivity-based control law, which is designed to dissipate energy from the robot’s dynamic system, facilitating the efficient driving of the actuator torques to the origin.

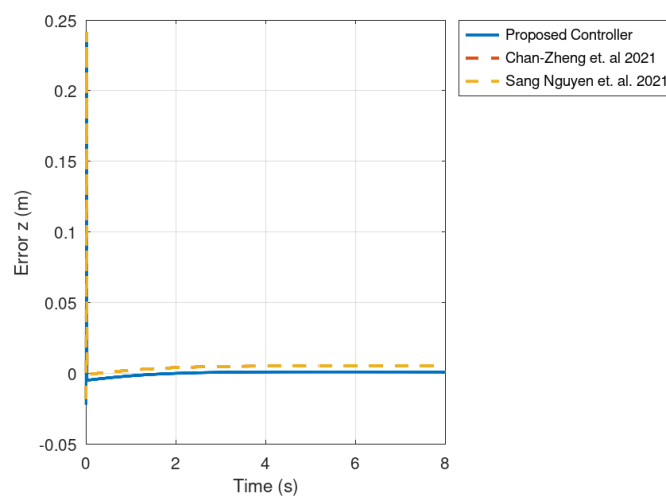
(a) Variable x (b) Variable y (c) Variable z **Figure 2.** Position of the robot in the x, y, z frames for the proposed strategy and [32,33].



(a) Error in x

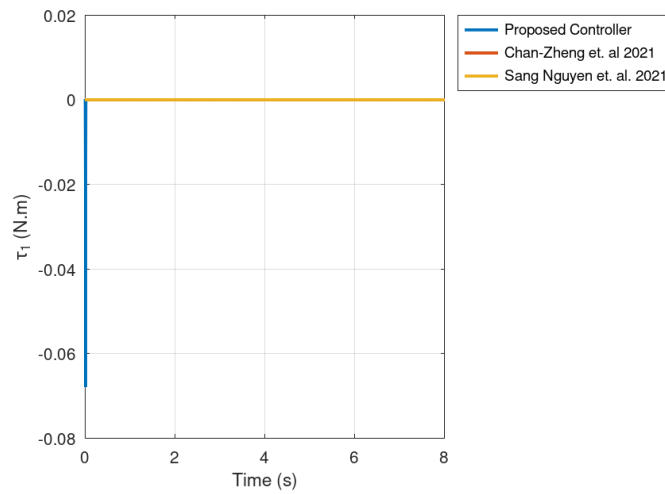
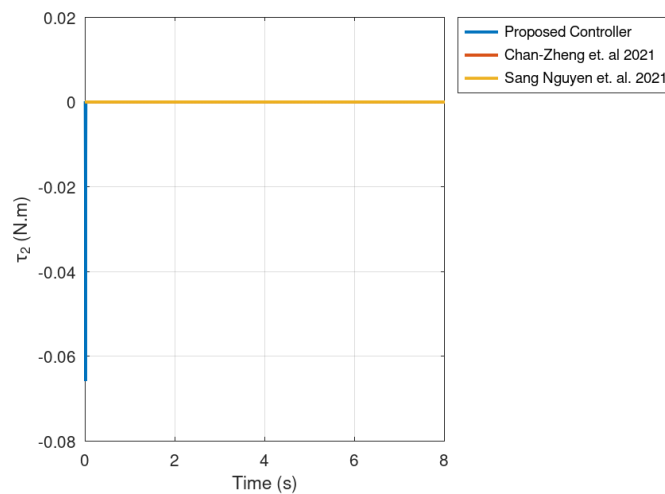
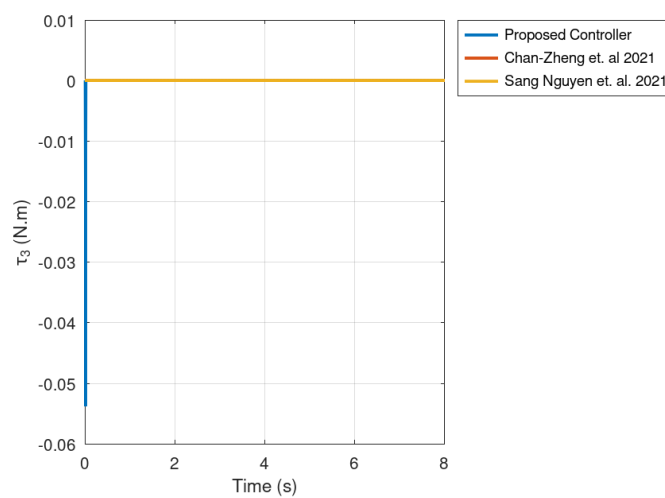


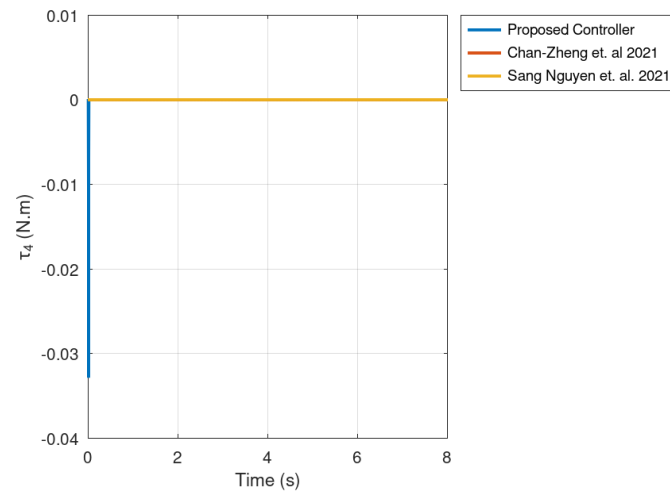
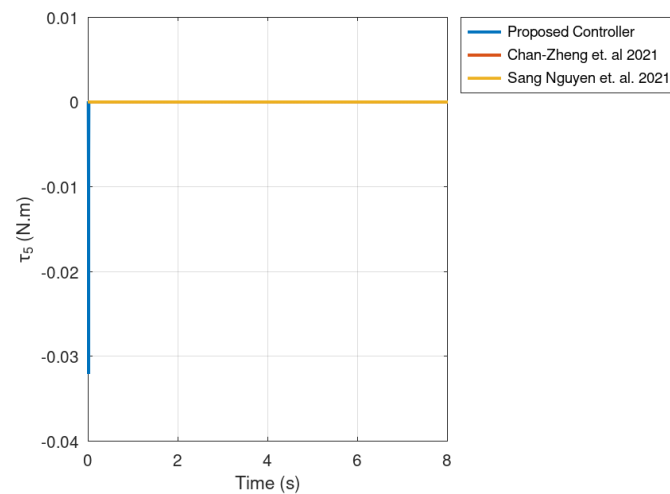
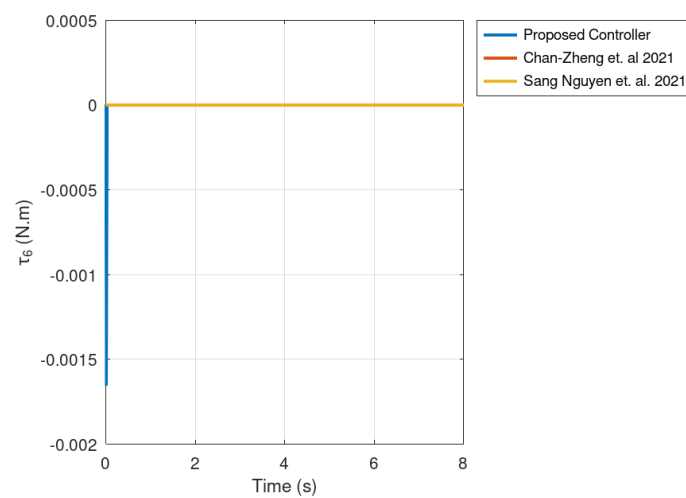
(b) Error in y



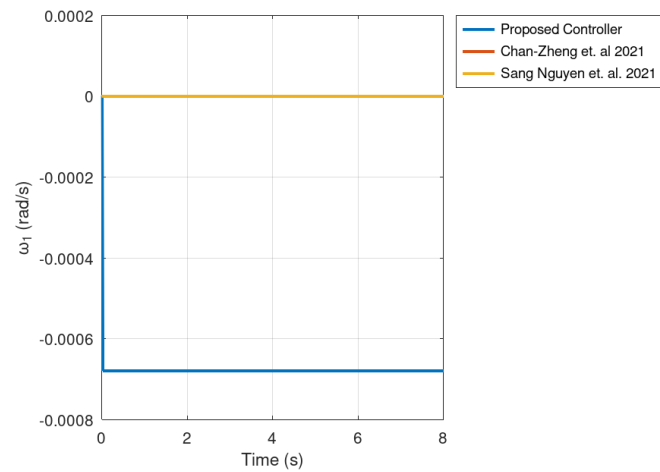
(c) Error in z

Figure 3. Position error of the robot in the x, y, z frames for the proposed strategy and [32,33].

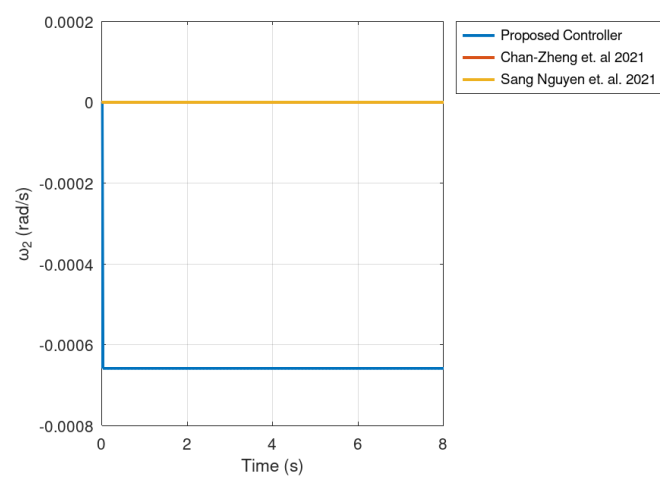
(a) Torque τ_1 (b) Torque τ_2 (c) Torque τ_3 **Figure 4.** Actuator torque $i = 1, 2, 3$ for experiment 1 for the proposed strategy and [32,33].

(a) Torque τ_4 (b) Torque τ_5 (c) Torque τ_6 **Figure 5.** Actuator torque $i = 4, 5, 6$ for experiment 1 for the proposed strategy and [32,33].

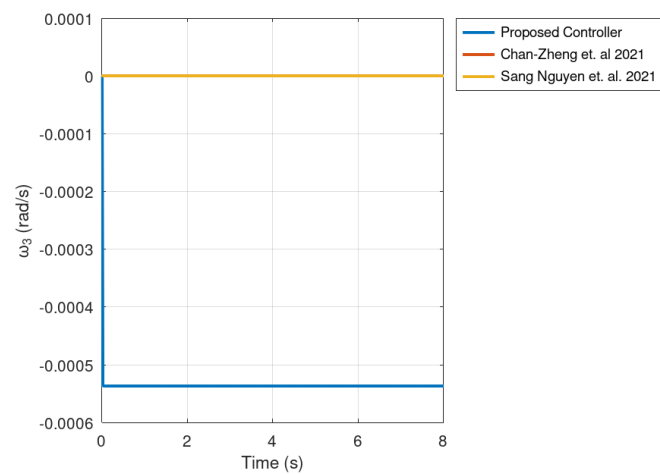
Then, in Figures 6 and 7, the angular velocities of the actuators are presented. These figures demonstrate that these variables reach the origin in finite time, with a considerably small velocity.



(a) Angular velocity ω_1

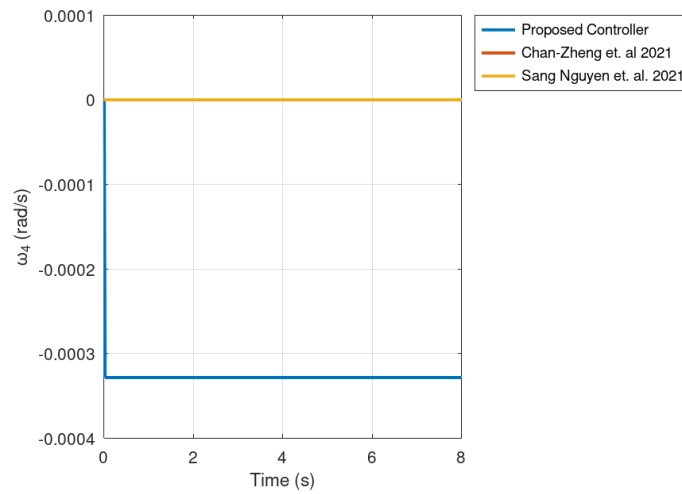


(b) Angular velocity ω_2

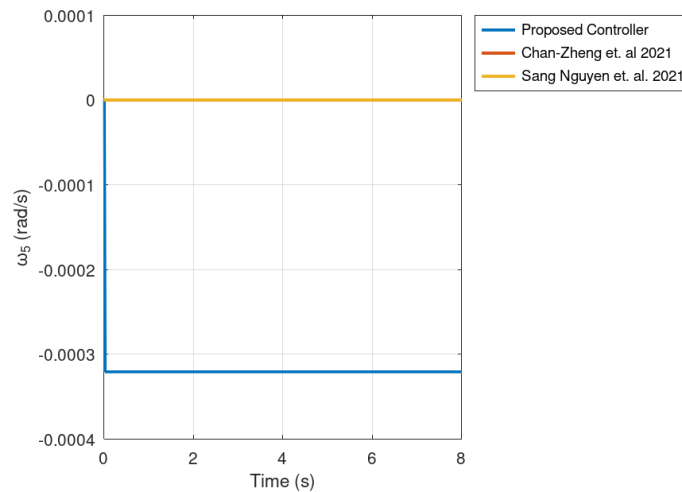


(c) Angular velocities ω_3

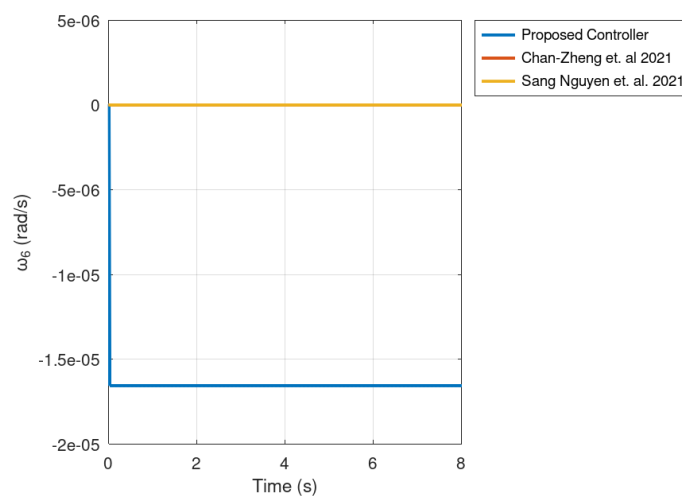
Figure 6. Actuator angular velocities ω_1 , ω_2 and ω_3 for the proposed strategy and [32,33].



(a) Velocity ω_4



(b) Velocity ω_5



(c) Angular velocity ω_6

Figure 7. Actuator angular velocities ω_4 , ω_5 and ω_6 for the proposed strategy and [32,33].

Finally, in Figure 8, the trajectory of the end effector in three dimensions is presented, observing how the reference trajectory is tracked accurately by the passivity-based controller for the robot Mitsubishi RV-3SB. This plot corroborates in three dimensions how the end effector is guided in a 3-D workspace. Table 4 presents the integral square error of the proposed control strategy in comparison with the proposed control strategies [32,33]. It is observed that the ISE obtained with the proposed control strategy for the variables x , y and z is smaller in comparison with the control strategies which appear in [32,33]. It is important to remark that the proposed control strategy provides similar results to the other two control strategies; however, it is important to highlight that in addition to the smaller integral square error (ISE) achieved using the proposed control strategy, the control effort is more suitable in comparison with the comparative approaches used in this benchmark.

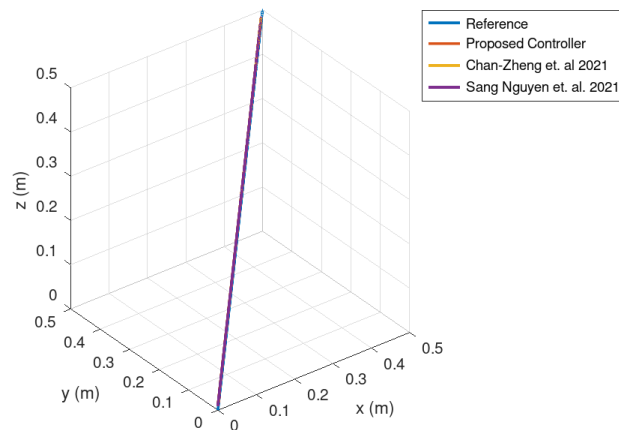


Figure 8. 3D trajectory of the robot RV-3SB for the proposed strategy and [32,33].

Table 4. Integral square error of experiment 1.

Controller Approach	ISE x	ISE y	ISE z
Proposed Controller	1.5957×10^{-2}	1.5457×10^{-2}	9.6052×10^{-3}
Chan Zheng et al., 2021 [32]	1.6341×10^{-2}	1.5863×10^{-2}	9.6887×10^{-3}
Nguyen et al., 2021 [33]	1.6341×10^{-3}	1.5863×10^{-2}	9.6887×10^{-3}

Finally, in Table 5, the correlation of the three variables x_1 , x_2 and x_3 with respect to their reference variables is presented. In this table, it is shown that the highest correlation is obtained with the proposed controller in comparison with the strategies shown in [32,33], proving that these variables reach the desired final value with more accuracy.

Table 5. Correlations between the reference variable and the proposed and comparative control strategies.

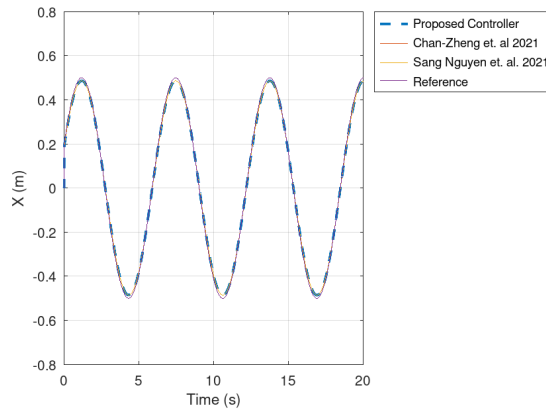
Controller Approach	Correlation x_1	Correlation x_2	Correlation x_3
Proposed Controller	0.9999	0.9965	0.9965
Chan Zheng et al., 2021 [32]	0.9998	0.9211	0.9229
Nguyen et al., 2021 [33]	0.9999	0.9964	0.9963

4.2. Experiment 2

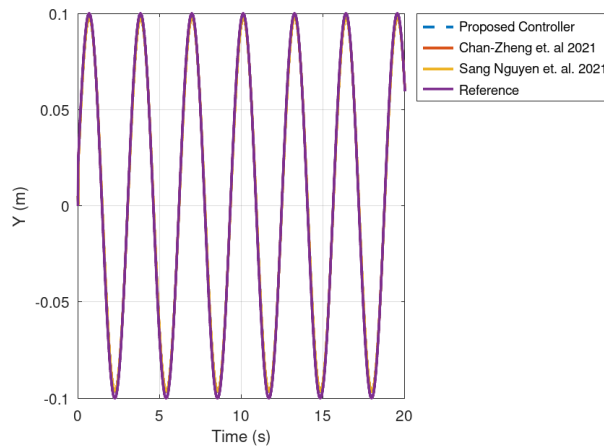
This numerical experiment is conducted similarly to Experiment 1 but with different conditions and trajectory generation. Its purpose is to validate and corroborate the theoretical results obtained during this research study.

In Figure 9, the end effector position of the Mitsubishi RV-3SB robot is obtained using the proposed control strategy and compared with the other two strategies used in this comparative benchmark [32,33]. It is evident that the results obtained with the proposed

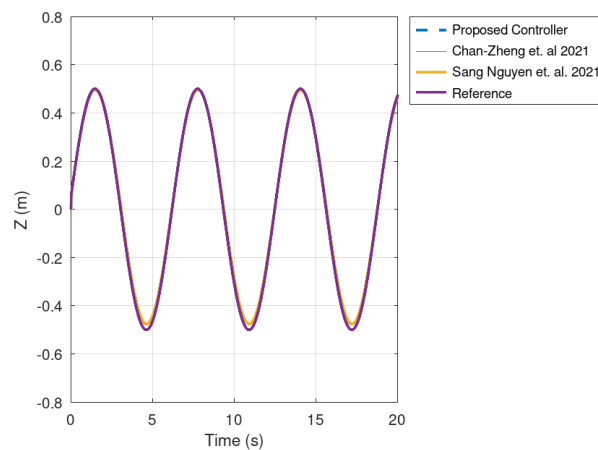
controller are optimal in comparison to those reported in [32,33]. In general, as verified later, the proposed strategy provides better results compared with the results obtained in [32,33].



(a) Variable x



(b) Variable y

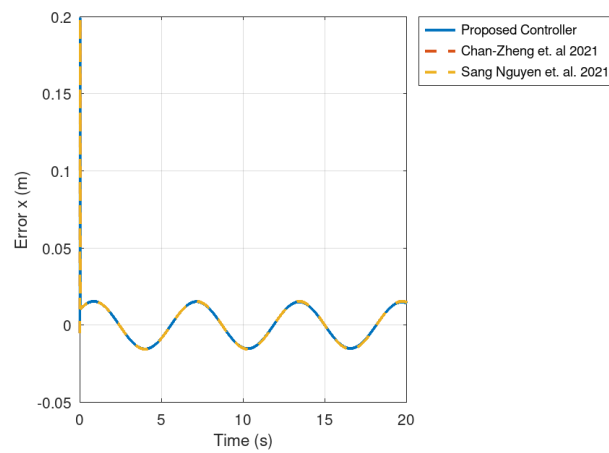


(c) Variable z

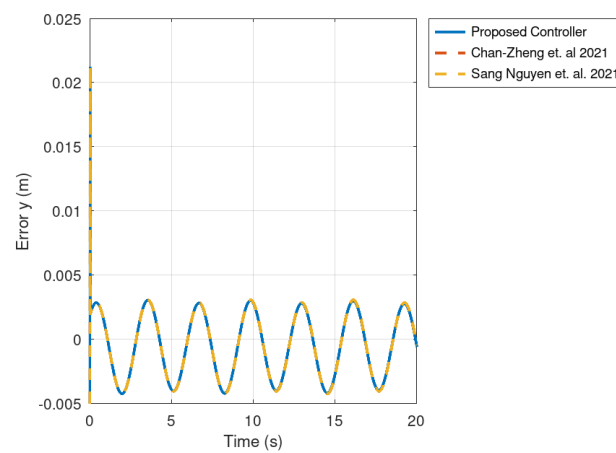
Figure 9. Position of the mobile robot in the x, y, z frames for the proposed strategy and [32,33].

Furthermore, in Figure 10, the error variables of the trajectory tracking of the end effector position of the RV-3SB robot are presented for the proposed control strategy, and they are compared with the strategies shown in [32,33]. It is observed that these error variables

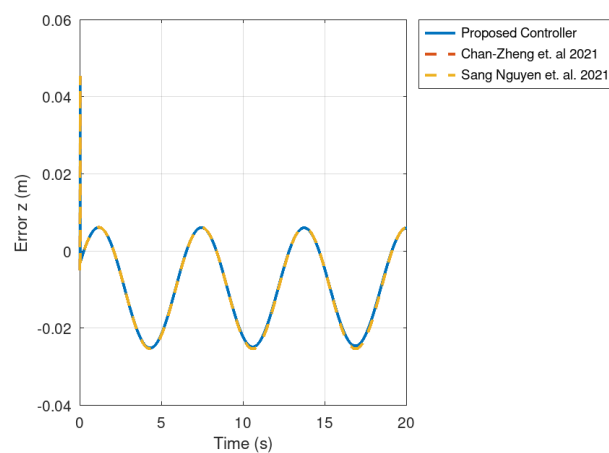
converge to the origin in finite time. Subsequently, it will be demonstrated that the results obtained using the proposed control strategy are more accurate compared with [32,33].



(a) Error in x



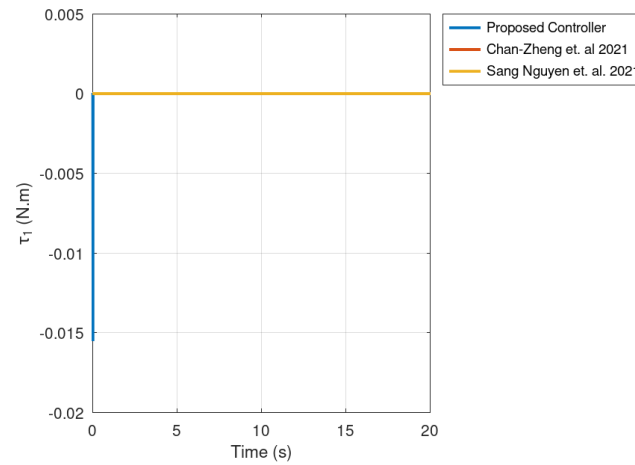
(b) Error in y



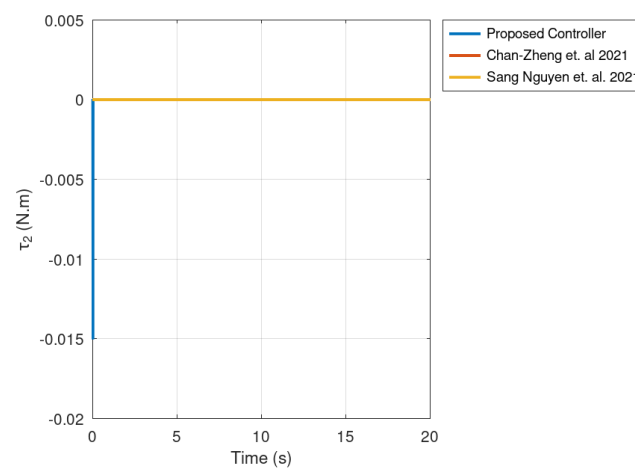
(c) Error in z

Figure 10. Position error of the mobile robot in the x, y, z frames for the proposed strategy and [32,33].

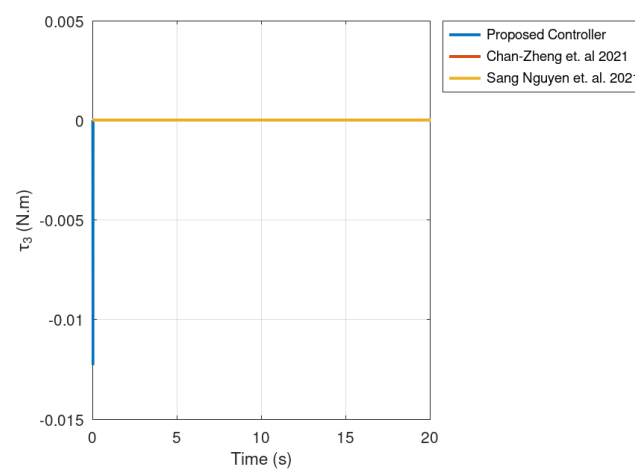
Then, Figures 11 and 12, show the actuator torques of the Mitsubishi RV-3SB robot, evincing that the actuator torque obtained using the proposed control strategy is significantly smaller compared to the actuator torque generated by the approaches depicted in [32,33].



(a) Torque τ_1

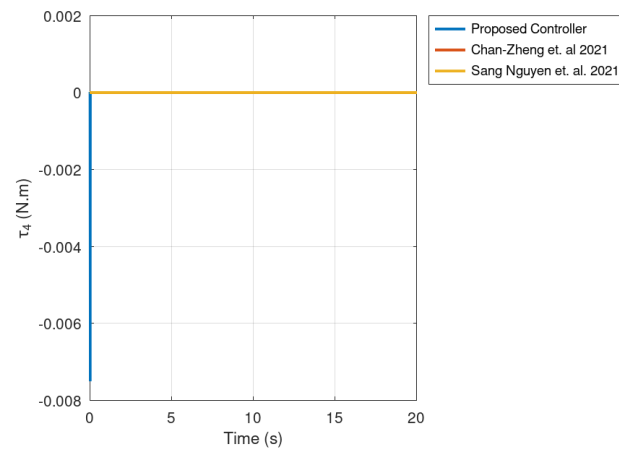
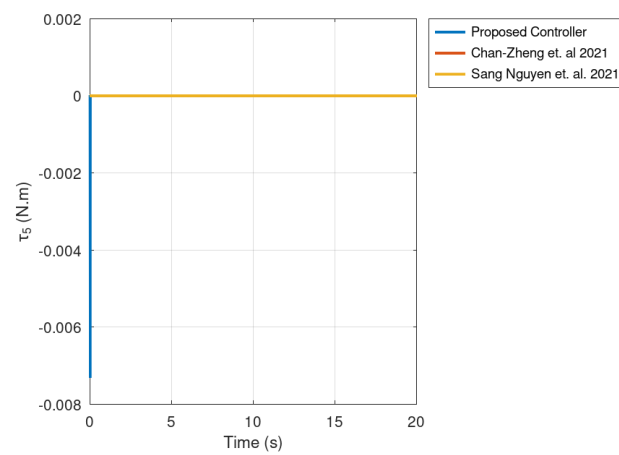
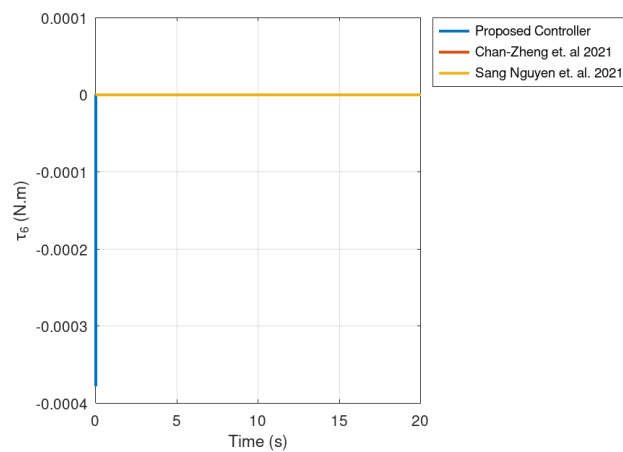


(b) Torque τ_2

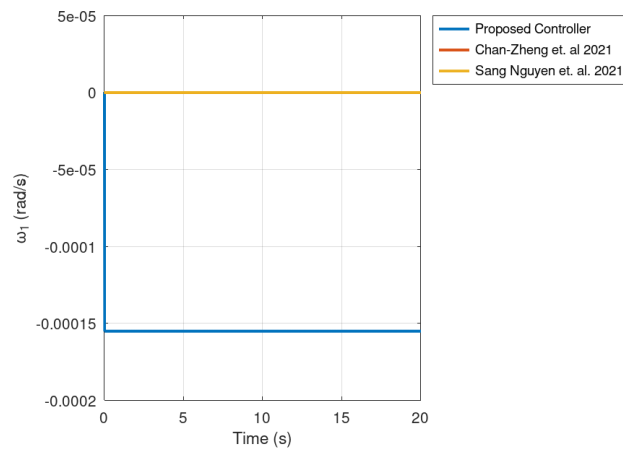


(c) Torque τ_3

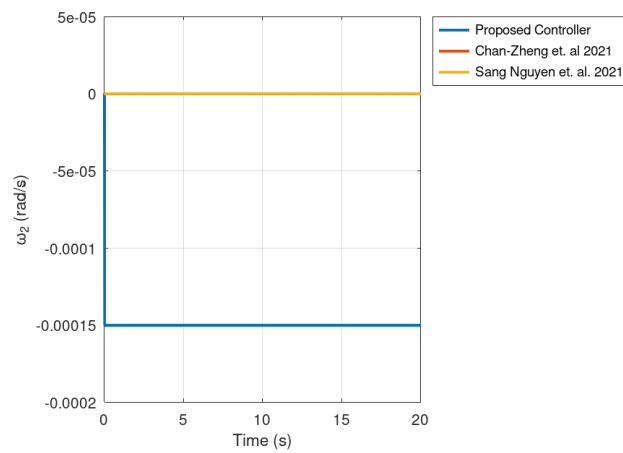
Figure 11. Actuator torque $i = 1, 2, 3$ for experiment 1 for the proposed strategy and [32,33].

(a) Torque τ_4 (b) Torque τ_5 (c) Torque τ_6 **Figure 12.** Actuator torque $i = 4, 5, 6$ for experiment 2 for the proposed strategy and [32,33].

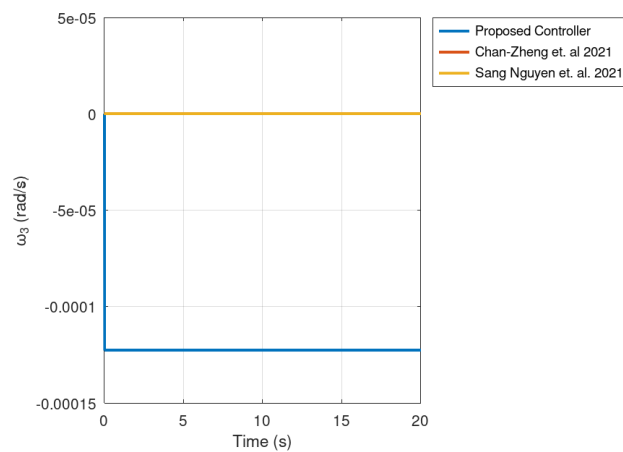
In Figures 13 and 14, the actuator angles generated using the proposed control strategy are compared with the strategies discussed in [32,33].



(a) Angular velocity ω_1

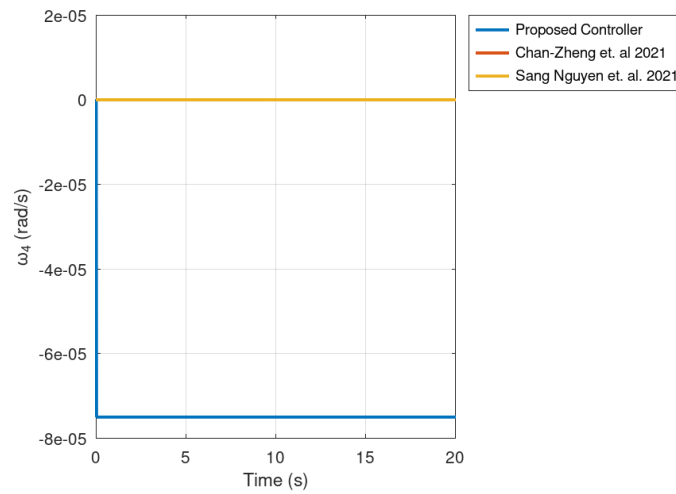


(b) Angular velocity ω_2

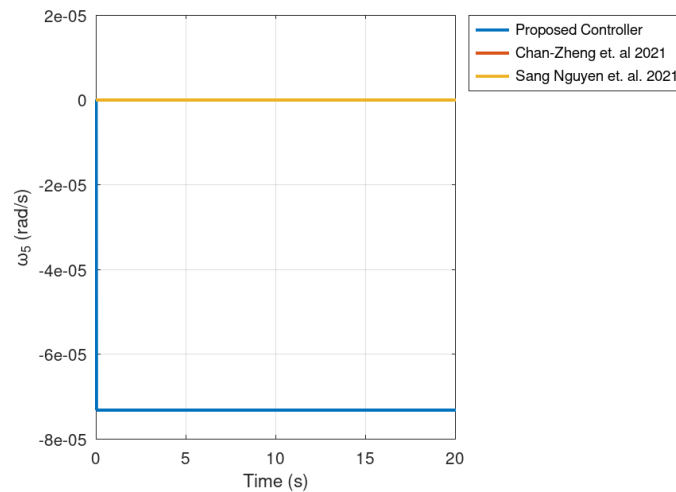


(c) Angular velocity ω_3

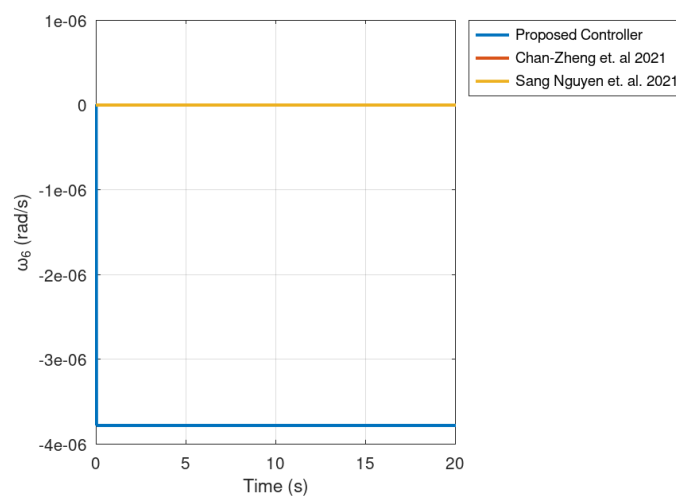
Figure 13. Actuator angular velocities ω_1 , ω_2 and ω_3 for the proposed strategy and [32,33].



(a) Velocity ω_4



(b) Velocity ω_5



(c) Angular velocity ω_6

Figure 14. Actuator angular velocities ω_4 , ω_5 and ω_6 for the proposed strategy and [32,33].

Finally, in Figure 15, the end effector trajectory of the Mitsubishi RV-3SB robot is evinced. The trajectory with the proposed controller is compared with the trajectory generated using the strategies shown in [32,33], proving that the results with the proposed controller are superior in comparison with the other strategies used in this benchmark.

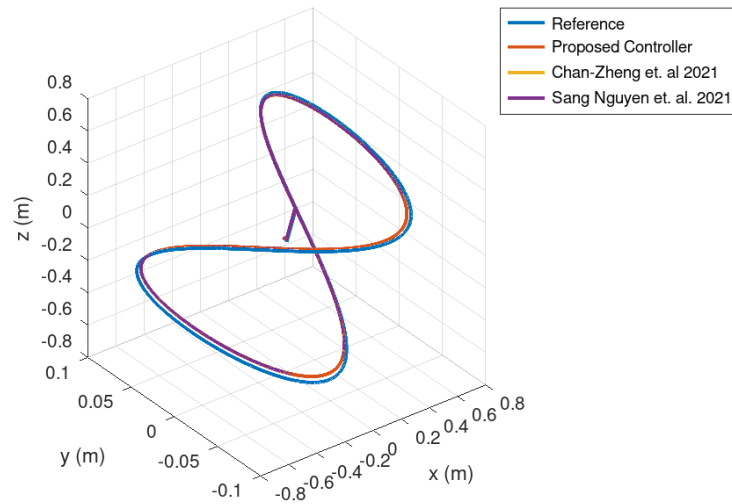


Figure 15. Three-dimensional trajectory of the robot RV-3SB for the proposed strategy and [32,33].

Finally, Table 6 presents the integral square error of the variables x , y and z . It is noticed that the ISE of the variables x , y and z for the proposed controller exhibits a small integral square error in comparison with the ISE of the strategies discussed in [32,33]. Despite these values are similar, the ISE obtained with the proposed control strategy is smaller.

Table 6. Integral square error of experiment 2.

Controller Approach	ISE x	ISE y	ISE z
Proposed Controller	1.1830×10^{-2}	2.5795×10^{-3}	1.4096×10^{-2}
Chan Zheng et al., 2021 [32]	1.2001×10^{-2}	2.6106×10^{-3}	1.4366×10^{-2}
Nguyen et al., 2021 [33]	1.2001×10^{-2}	2.6106×10^{-3}	1.4366×10^{-2}

Similar to experiment 1, Table 7 shows the correlations of the variables x_1 , x_2 and x_3 in relation to the reference variables. It is verified in this table that the highest correlation is obtained with the proposed controller. This means that the proposed controller yields a steady state error that is minimal in comparison with other controllers [32,33].

Table 7. Correlations between the reference variable and the proposed and comparative control strategies.

Controller Approach	Correlation x_1	Correlation x_2	Correlation x_3
Proposed Controller	0.9999	0.9965	0.9965
Chan Zheng et al., 2021 [32]	0.9998	0.9211	0.9229
Nguyen et al., 2021 [33]	0.9999	0.9964	0.9963

5. Discussion

In this research study, a novel passivity-based controller for the Mitsubishi RV-3SB robot is theoretically and experimentally demonstrated. Considering that this robot is used experimentally in laboratories in universities around the world, one of the main contributions of this research study is that the kinematics, dynamics, and control of this robot have not been determined before. The dynamics of the robot are obtained using the Euler–Lagrange approach, considering the tractability of the problem. It is important to

mention that the selected passivity-based controller is selected due to its relative simplicity, energy considerations, and easy implementation. The passivity-based controller is designed by implementing an appropriate storage function in order to identify the passivity control law and to stabilize the system variable. Theoretically, the passivity-based controller is well suited to trajectory tracking, as the stability conditions of the controller are fulfilled to drive the system's energy towards zero.

It is important to note that the numerical experiment section conducted two experiments, calculating the integral square error of the variables x , y and z to verify that the tracking error adheres as closely as possible to the origin in finite time. A drawback observed in these two numerical experiments is the necessity for the integral square error (ISE) to be minimized. It is important to mention that to solve this, as verified in experiment 1, the gains of the controllers must be selected as long as they are positive definite. This condition ensures the stability of the error dynamics, but at the same time, as proved in experiment 2, the error can be driven accurately to zero by implementing a tuning or optimization algorithm. This issue will be improved in future research studies, considering that the stability of the tracking error is minimized accurately only by selecting a positive definite gain.

6. Conclusions

In this research study, a passivity-based controller for the Mitsubishi RV-3SB robot is synthesized. Considering that many laboratories in universities around the world implement this robot mechanism for academic or research purposes, it is crucial to design a novel but, at the same time, implementable controller in order to drive the error variable with its dynamics to zero in finite time. Taking advantage of the energy considerations of passivity-based controllers, a relatively simple control law is obtained, taking into consideration that the resulting controller must be implementable in affordable hardware, independently if it is a small laboratory with lack of equipment.

To design the passivity-based controller, a storage function was employed to derive the necessary control law. Subsequently, two numerical experiments were conducted to validate the theoretical findings and confirm the trajectory tracking performance. The goal of these experiments was to ensure that the error variables of the end effector approach the origin within finite time, all while maintaining a minimal integral square error. This rigorous validation process serves to corroborate the effectiveness and robustness of the proposed passivity-based control strategy.

Author Contributions: Conceptualization, F.E.S., C.E.G.C. and M.C.; methodology, F.E.S.; software, F.E.S.; validation, M.C. formal analysis, F.E.S.; investigation, F.E.S., C.E.G.C. and M.C.; resources, C.E.G.C. and M.C.; data curation, F.E.S.; writing—original draft preparation, F.E.S., C.E.G.C. and M.C.; writing—review and editing, F.E.S., C.E.G.C. and M.C.; visualization, C.E.G.C. and M.C.; supervision, C.E.G.C. and M.C.; project administration, C.E.G.C. and M.C.; funding acquisition, M.C. All authors have read and agreed to the published version of the manuscript.

Funding: This research was funded by the Universidad Don Bosco, El Salvador.

Data Availability Statement: Not applicable.

Conflicts of Interest: The authors declare no conflict of interest.

References

1. Chen, F.; Ju, H.; Liu, X. Inverse kinematic formula for a new class of 6R robotic arms with simple constraints. *Mech. Mach. Theory* **2023**, *179*, 105118. [[CrossRef](#)]
2. Xu, K.; Chen, H.; Mueller, A.; Ding, X. Kinematics of the center of mass for robotic mechanisms based on lie group theory. *Mech. Mach. Theory* **2022**, *175*, 104933. [[CrossRef](#)]
3. Shrey, S.; Patil, S.; Pawar, N.; Lokhande, C.; Dandage, A.; Ghorpade, R.R. Forward kinematic analysis of 5-DOF LYNX6 robotic arm used in robot-assisted surgery. *Mater. Today Proc.* **2022**, *72*, 858–863. [[CrossRef](#)]

4. Yang, B.; Yang, W. Modular approach to kinematic reliability analysis of industrial robots. *Reliab. Eng. Syst. Saf.* **2023**, *229*, 108841. [[CrossRef](#)]
5. Cardona, M. A new approach for the forward kinematics of general stewart-gough platforms. In Proceedings of the 2015 IEEE Thirty Fifth Central American and Panama Convention (CONCAPAN XXXV), Tegucigalpa, Honduras, 11–13 November 2015; pp. 1–6.
6. Wang, X.; Sun, S.; Zhang, P.; Wu, M.; Zhao, C.; Zhang, D.; Meng, X. Model-based kinematic and non-kinematic calibration of a 7R 6-DOF robot with non-spherical wrist. *Mech. Mach. Theory* **2022**, *178*, 105086. [[CrossRef](#)]
7. Yin, F.; Wang, L.; Tian, W.; Zhang, X. Kinematic calibration of a 5-DOF hybrid machining robot using an extended Kalman filter method. *Precis. Eng.* **2023**, *79*, 86–93. [[CrossRef](#)]
8. Zhao, Y.; Fang, H.; Diao, B.; Zhang, X.; Xu, J. Exploiting the bistable dynamics in a two-module vibration-driven robot for locomotion performance enhancement. *J. Sound Vib.* **2023**, *544*, 117387. [[CrossRef](#)]
9. Misyurin, S.; Nosova, N.; Nelyubin, A.; Zhao, J.; Martins, D. Hexabot Robot: Derivation of the dynamics equations. *Procedia Comput. Sci.* **2022**, *213*, 680–687. [[CrossRef](#)]
10. Yu, P.; Tan, N.; Zhong, Z. Comparative studies and performance analysis on neural-dynamics-driven control of redundant robot manipulators with unknown models. *Eng. Appl. Artif. Intell.* **2023**, *117*, 105528. [[CrossRef](#)]
11. Lages, W.F. Remote Teaching of Dynamics and Control of Robots Using ROS 2. *IFAC-PapersOnLine* **2022**, *55*, 279–284. [[CrossRef](#)]
12. Ba, K.; Song, Y.; Yu, B.; He, X.; Huang, Z.; Li, C.; Yuan, L.; Kong, X. Dynamics compensation of impedance-based motion control for LHDS of legged robot. *Robot. Auton. Syst.* **2021**, *139*, 103704. [[CrossRef](#)]
13. Zhao, L.; Li, J.; Li, H.; Liu, B. Double-loop tracking control for a wheeled mobile robot with unmodeled dynamics along right angle roads. *ISA Trans.* **2022**, *136*, 525–534. [[CrossRef](#)]
14. Gallardo-Alvarado, J.; Gallardo-Razo, J. Chapter 18—Fundamentals of screw theory. In *Mechanisms*; Gallardo-Alvarado, J., Gallardo-Razo, J., Eds.; Emerging Methodologies and Applications in Modelling, Identification and Control; Academic Press: Cambridge, MA, USA, 2022; pp. 381–420.
15. Cibicik, A.; Egeland, O. Dynamic modelling and force analysis of a knuckle boom crane using screw theory. *Mech. Mach. Theory* **2019**, *133*, 179–194. [[CrossRef](#)]
16. Shi, C.; Guo, H.; Zhang, S.; Liu, R.; Deng, Z. Configuration synthesis of linear foldable over-constrained deployable unit based on screw theory. *Mech. Mach. Theory* **2021**, *156*, 104163. [[CrossRef](#)]
17. Kang, X.; Feng, H.; Dai, J.S.; Yu, H. High-order based revelation of bifurcation of novel Schatz-inspired metamorphic mechanisms using screw theory. *Mech. Mach. Theory* **2020**, *152*, 103931. [[CrossRef](#)]
18. Fan, S.; Shen, G.; Liu, T.; Lan, W.; Song, G. A universal modelling approach and a response index to the vibration analysis for space parallel robots by means of screw theory. *Appl. Math. Model.* **2023**, *114*, 1–22. [[CrossRef](#)]
19. Cai, J.; Deng, X.; Feng, J.; Xu, Y. Mobility analysis of generalized angulated scissor-like elements with the reciprocal screw theory. *Mech. Mach. Theory* **2014**, *82*, 256–265. [[CrossRef](#)]
20. Xu, M.; Wang, J. Learning strategy for continuous robot visual control: A multi-objective perspective. *Knowl.-Based Syst.* **2022**, *252*, 109448. [[CrossRef](#)]
21. Korayem, M.; Vosoughi, R.; Vahidifar, V. Design, manufacture, and control of a laparoscopic robot via Leap Motion sensors. *Measurement* **2022**, *205*, 112186. [[CrossRef](#)]
22. Wang, M.; Li, W.; Luo, J.; Walter, U. Coordinated hierarchical control of space robotic safe manipulation with load sharing. *Acta Astronaut.* **2023**, *202*, 360–372. [[CrossRef](#)]
23. Mujica, M.; Crespo, M.; Benoussaad, M.; Junco, S.; Fourquet, J.Y. Robust variable admittance control for human–robot co-manipulation of objects with unknown load. *Robot. Comput.-Integr. Manuf.* **2023**, *79*, 102408. [[CrossRef](#)]
24. Jafari, M.; Mobayen, S.; Bayat, F.; Roth, H. A nonsingular terminal sliding algorithm for swing and stance control of a prosthetic leg robot. *Appl. Math. Model.* **2023**, *113*, 13–29. [[CrossRef](#)]
25. Bhandari, G.; Raj, R.; Pathak, P.M.; Yang, J.M. Robust control of a planar snake robot based on interval type-2 Takagi–Sugeno fuzzy control using genetic algorithm. *Eng. Appl. Artif. Intell.* **2022**, *116*, 105437. [[CrossRef](#)]
26. de Jong, M.C.; Kosaraju, K.C.; Scherpen, J.M. On control of voltage-actuated piezoelectric beam: A Krasovskii passivity-based approach. *Eur. J. Control* **2022**, *69*, 100724. [[CrossRef](#)]
27. Zhou, J.; Zhang, Q.; Hassan, M.A.; Zhang, Z.; Hou, M.; Wu, S.; Li, Y.; Li, E.; Guerrero, J.M. A robust passivity based model predictive control for buck converter supplying constant power load. *Energy Rep.* **2021**, *7*, 792–813. [[CrossRef](#)]
28. Gandarilla, I.; Santibáñez, V.; Sandoval, J.; Romero, J.G. PID passivity-based control laws for joint position regulation of a self-balancing robot. *Control Eng. Pract.* **2021**, *116*, 104927. [[CrossRef](#)]
29. Zhang, S.; Zhu, H.; He, X.; Feng, Y.; Pang, C.K. Passivity-based coupling control for underactuated three-dimensional overhead cranes. *ISA Trans.* **2022**, *126*, 352–360. [[CrossRef](#)] [[PubMed](#)]
30. Shen, P.Y.; Schatz, J.; Caverly, R.J. Passivity-based adaptive trajectory control of an underactuated 3-DOF overhead crane. *Control Eng. Pract.* **2021**, *112*, 104834. [[CrossRef](#)]
31. Shahna, M.H.; Abedi, M. Design of a finite time passivity based adaptive sliding mode control implementing on a spacecraft attitude dynamic simulator. *Control Eng. Pract.* **2021**, *114*, 104866. [[CrossRef](#)]

32. Chan-Zheng, C.; Borja, P.; Scherpen, J.M. Passivity-based control of mechanical systems with linear damping identification. *IFAC-PapersOnLine* **2021**, *54*, 255–260. [[CrossRef](#)]
33. Nguyen, T.S.; Hoang, N.H.; Tan, C.K.; Bin Hussain, M.A. Proportional-Integral passivity-based control design of perturbed non-standard Hamiltonian systems. *IFAC-PapersOnLine* **2021**, *54*, 19–24. [[CrossRef](#)]
34. Benamar, F.; Bidaud, P.; Le Menn, F. Generic differential kinematic modeling of articulated mobile robots. *Mech. Mach. Theory* **2010**, *45*, 997–1012. [[CrossRef](#)]
35. Tsai, Y.; Soni, A. Workspace synthesis of 3R, 4R, 5R and 6R robots. *Mech. Mach. Theory* **1985**, *20*, 555–563. [[CrossRef](#)]
36. Hon-Cheung, Y. Four co-reciprocal screws and their kinematic significance. *Mech. Mach. Theory* **1987**, *22*, 199–203. [[CrossRef](#)]
37. Yukhimets, D.A.; Gubankov, A.S. Method of identification of kinematic and elastostatic parameters of multilink manipulators without external measuring devices. *IFAC-PapersOnLine* **2020**, *53*, 9879–9884. [[CrossRef](#)]
38. Guglielmetti, P.; Longchamp, R. Task Space Control of the Delta Parallel Robot. *IFAC Proc. Vol.* **1992**, *25*, 337–342. [[CrossRef](#)]
39. Guglielmetti, P.; Longchamp, R. A closed form inverse dynamics model of the delta parallel robot. *IFAC Proc. Vol.* **1994**, *27*, 51–56. [[CrossRef](#)]
40. Shahidi, A.; Hüsing, M.; Corves, B. Kinematic Control of Serial Manipulators Using Clifford Algebra. *IFAC-PapersOnLine* **2020**, *53*, 9992–9999. [[CrossRef](#)]
41. Liu, H.; Kecskeméthy, A.; Huang, T. An automatic approach for identification of natural reciprocal screw systems of serial kinematic chains based on the invariance properties matrix. *Mech. Mach. Theory* **2017**, *107*, 352–368. [[CrossRef](#)]
42. Abaunza, H.; Chandra, R.; Özgür, E.; Ramón, J.A.C.; Mezouar, Y. Kinematic screws and dual quaternion based motion controllers. *Control Eng. Pract.* **2022**, *128*, 105325. [[CrossRef](#)]
43. Zaplana, I.; Hadfield, H.; Lasenby, J. Closed-form solutions for the inverse kinematics of serial robots using conformal geometric algebra. *Mech. Mach. Theory* **2022**, *173*, 104835. [[CrossRef](#)]
44. Kolathaya, S. Local stability of PD controlled bipedal walking robots. *Automatica* **2020**, *114*, 108841. [[CrossRef](#)]
45. Nicosia, S.; Tomei, P. Model reference adaptive control algorithms for industrial robots. *Automatica* **1984**, *20*, 635–644. [[CrossRef](#)]
46. Huang, J.; Wen, C.; Wang, W.; Jiang, Z.P. Adaptive output feedback tracking control of a nonholonomic mobile robot. *Automatica* **2014**, *50*, 821–831. [[CrossRef](#)]
47. Xin, X.; Liu, Y. Reduced-order stable controllers for two-link underactuated planar robots. *Automatica* **2013**, *49*, 2176–2183. [[CrossRef](#)]
48. Perrusquía, A.; Garrido, R.; Yu, W. Stable robot manipulator parameter identification: A closed-loop input error approach. *Automatica* **2022**, *141*, 110294. [[CrossRef](#)]
49. Behera, P.; Dey, A.; Patra, S. Control of negative imaginary systems exploiting a dissipative characterization. *Automatica* **2022**, *146*, 110634. [[CrossRef](#)]
50. Faulwasser, T.; Kellett, C.M. On continuous-time infinite horizon optimal control—Dissipativity, stability, and transversality. *Automatica* **2021**, *134*, 109907. [[CrossRef](#)]
51. Xue, M.; Yan, H.; Zhang, H.; Wang, M.; Zhang, D. Dissipative output feedback tracking control of Markov jump systems under compensation scheme. *Automatica* **2022**, *146*, 110535. [[CrossRef](#)]
52. Faulwasser, T.; Kellett, C.M. Dissipativity in Infinite-Horizon Optimal Control: Willems’ 1971 Paper Revisited. *IFAC-PapersOnLine* **2022**, *55*, 49–54. [[CrossRef](#)]
53. Adhira, B.; Nagamani, G.; Dafik, D. Non-fragile extended dissipative synchronization control of delayed uncertain discrete-time neural networks. *Commun. Nonlinear Sci. Numer. Simul.* **2023**, *116*, 106820. [[CrossRef](#)]
54. Neves, L.C.; Paim, G.V.; Queindec, I.; Moreno, U.F.; De Pieri, E.R. Passivity and Power Based Control of a Robot with Parallel Architecture. *IFAC Proc. Vol.* **2011**, *44*, 14608–14613. [[CrossRef](#)]
55. Leite, A.C.; Cruz, F.L.; Lizarralde, F. Adaptive Passivity-based Hybrid Pose/Force Control for Uncertain Robots. *IFAC-PapersOnLine* **2020**, *53*, 3854–3860. [[CrossRef](#)]
56. Sakai, S.; Stramigioli, S. Passivity based force control of hydraulic robots. *IFAC Proc. Vol.* **2009**, *42*, 20–25. [[CrossRef](#)]
57. Nguyen, T.; Hatanaka, T.; Doi, M.; Garone, E.; Fujita, M. A Passivity-Based Distributed Reference Governor for Constrained Robotic Networks. *IFAC-PapersOnLine* **2017**, *50*, 15434–15439. [[CrossRef](#)]
58. Spong, M.W. Some new results in passivity based control of robots. In Proceedings of the 6th IFAC Symposium on Nonlinear Control Systems 2004 (NOLCOS 2004), Stuttgart, Germany, 1–3 September 2004; Volume 37, pp. 33–40.
59. Hu, J.; Lennox, B.; Arvin, F. Robust formation control for networked robotic systems using Negative Imaginary dynamics. *Automatica* **2022**, *140*, 110235. [[CrossRef](#)]
60. Sanchez, M.; Cruz-Ortiz, D.; Ballesteros, M.; Salgado, I.; Chairez, I. Output feedback robust control for teleoperated manipulator robots with different workspace. *Expert Syst. Appl.* **2022**, *206*, 117838. [[CrossRef](#)]
61. Niu, S.; Chen, W.H.; Lu, X. Sliding mode control with integral sliding surface for linear uncertain impulsive systems with time delays. *Appl. Math. Model.* **2023**, *113*, 439–455. [[CrossRef](#)]
62. Sami, I.; Ro, J.S. Adaptive supertwisting sliding mode control of multi-converter MVDC power systems. *Energy Rep.* **2022**, *8*, 467–479. [[CrossRef](#)]

63. Pal, P.; Jin, G.G.; Bhakta, S.; Mukherjee, V. Adaptive chaos synchronization of an attitude control of satellite: A backstepping based sliding mode approach. *Heliyon* **2022**, *8*, e11730. [[CrossRef](#)] [[PubMed](#)]
64. Cardona, M.; Garzón-Castro, C.L.; Gutiérrez, S. Kinematics Solution of the RV-3SB Robot Using Successive Screws. In Proceedings of the 2020 IEEE ANDESCON, Quito, Ecuador, 13–16 October 2020; pp. 1–6.

Disclaimer/Publisher's Note: The statements, opinions and data contained in all publications are solely those of the individual author(s) and contributor(s) and not of MDPI and/or the editor(s). MDPI and/or the editor(s) disclaim responsibility for any injury to people or property resulting from any ideas, methods, instructions or products referred to in the content.